Thiede, J., Myhre, A.M., Firth, J.V., Johnson, G.L., and Ruddiman, W.F. (Eds.), 1996
Proceedings of the Ocean Drilling Program, Scientific Results, Vol. 151

26. LATE QUATERNARY STABLE ISOTOPIC STRATIGRAPHY OF HOLE 910A, YERMAK PLATEAU, ARCTIC OCEAN: RELATIONS WITH SVALBARD/BARENTS SEA ICE SHEET HISTORY[1]

Benjamin P. Flower[2]

ABSTRACT

Ocean Drilling Program Hole 910A on the Yermak Plateau (80°N, 5°E) at 552 m water depth provides one of the first opportunities for high-resolution studies of Quaternary Arctic Ocean climates. Oxygen and carbon isotopic data based on *Neogloboquadrina pachyderma* (sinistrally coiling) from the top 24.5 m at 10 cm sampling resolution provide both stratigraphic age control and a history of middle through late Quaternary surface water environments. The $\delta^{18}O$ data reveal oxygen isotope Stages 1 through 16 (and possibly 17), with an amplitude of ~1‰. Carbon isotopic values in the section from ~19.5 to 24.5 m below seafloor (mbsf) exhibit a series of ~1‰ fluctuations, followed by a permanent 1‰ increase at ~19.5 mbsf. Above ~19.5 mbsf, $\delta^{13}C$ values are relatively stable, except for large spikes of ~0.5‰, mainly during inferred interglacials. Significantly, the section from ~19.5 to 24.5 mbsf is a remarkable "overconsolidated section," marked by high values for bulk density and sediment strength. The large variations in $\delta^{13}C$ below ~19.5 mbsf, and the overconsolidated nature of the section, suggest a fundamentally different sedimentary environment. Possible explanations include (1) episodic grounding of a marine-based ice sheet, perhaps derived from the Barents Sea ice sheet and buttressed by Svalbard, which overcompacted the sediment and strongly influenced surface water chemistry on the Yermak Plateau, and/or (2) coarser grained glacial sedimentation that allowed enhanced compaction during this interval. Oxygen isotopic stratigraphy suggests that overconsolidation ended near the Stage 17/16 boundary (~670 ka), reflecting a major change in state of the Svalbard/Barents Sea ice sheet.

INTRODUCTION

The Yermak Plateau is an aseismic topographic marginal high about 100 km north of Svalbard. The plateau is an Eocene (?) volcanic edifice, although basement has not been drilled and, consequently, the age is not well known. The Yermak Plateau lies just north of the Arctic Gateway at the Fram Strait, which connects the Arctic Ocean and the Norwegian-Greenland Sea. The Yermak Plateau is seasonally ice free in the present day, as a result of warm waters from the West Spitsbergen Current (WSC). This current is an extension of the warm Norwegian Current that splits south of Svalbard into a western branch (the WSC, flowing through the Fram Strait) and an eastern branch (flowing through the Barents Sea) into the Arctic Ocean.

Low sea-ice conditions in the summer of 1993 allowed the *JOIDES Resolution* to drill at three sites in a depth transect on the Yermak Plateau. Sites 910, 911, and 912 were drilled at 552, 902, and 1037 m water depth (mwd), respectively, during Ocean Drilling Program (ODP) Leg 151 (Fig. 1). Sediments recovered at Site 910 (80°16′N, 6°35′E) range in age from late Pliocene (in Hole 910C only) to Holocene; the total depth drilled was 506 m below seafloor (mbsf). The sediments are nearly homogeneous, dominantly fine-grained silty clays, with a large ice-rafted debris (IRD) fraction. Carbonate material was sparse, partly because of dilution by terrestrially derived material. Dropstones were found throughout the sequence, attesting to a high flux of debris-laden icebergs (Myhre, Thiede, Firth, et al., 1995). Recovery in the Quaternary at Hole 910A was nearly 100% from 0 to 24.5 mbsf, with good magnetostratigraphic and biostratigraphic age control (Shipboard Scientific Party, 1995; Sato and Kameo, this volume).

Drilling in Hole 910A was inhibited by an "overconsolidated section" below ~19.5 mbsf, marked by large increases downcore in wet-bulk density, from ~1.3 to 1.7 g/cm^3, and in sediment strength, from ~150 to 300 mPa (Site 910; Shipboard Scientific Party, 1995). Sediment strength increased gradually from ~16 to 19 mbsf and rapidly

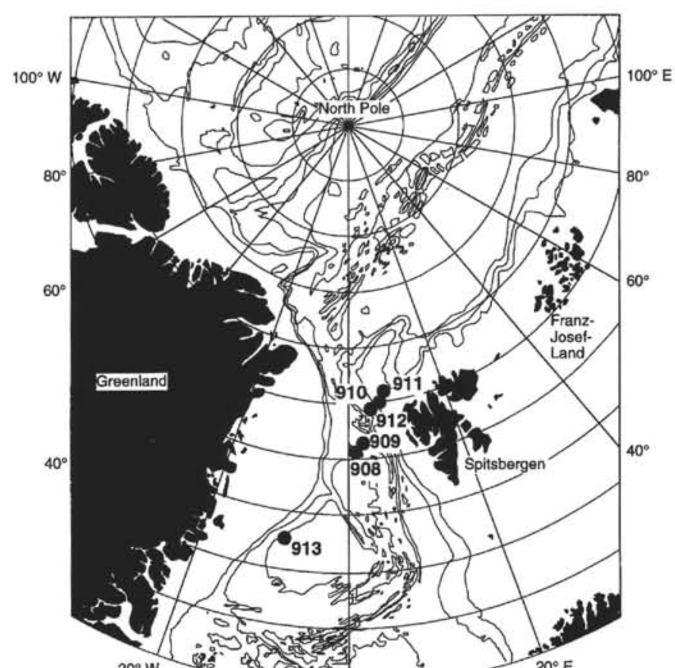

Figure 1. Location map of the Arctic Gateway region showing Leg 151 drill sites and important basins and ridges in the area. Sites 910, 911, and 912 are on the Yermak Plateau at ~80°N. Bathymetric contour interval is 1000 m.

[1]Thiede, J., Myhre, A.M., Firth, J.V., Johnson, G.L., and Ruddiman, W.F. (Eds.), 1996. *Proc. ODP, Sci. Results,* 151: College Station, TX (Ocean Drilling Program).
[2]Institute of Marine Sciences and Earth Sciences Board, University of California, Santa Cruz, Santa Cruz, CA 95064, U.S.A. flower@earthsci.ucsc.edu

centered at 19.5 mbsf. On board ship, this section was classified as silty clays to clayey silts. The thickness of this section is not well known because of core recovery problems below ~35 mbsf; the base is known to be between ~70 and 95 mbsf (Site 910; Shipboard Scientific Party, 1995). Only limited increases in consolidation were observed in the upper parts of Site 911 (902 mwd) and Site 912 (1037 mwd) on the Yermak Plateau. Also, Site 910 seismic stratigraphy revealed an acoustically chaotic upper section, whereas seismic sections at Sites 911 and 912 are well stratified (Myhre, Thiede, Firth, et al., 1995).

Interpretations by the Leg 151 Shipboard Scientific Party for the cause of the remarkable overconsolidated section at Site 910 include (1) grounding of a marine-based ice sheet, perhaps derived from the Barents Sea ice sheet and buttressed by Svalbard, and/or (2) coarser-grained glacial sedimentation that enhanced compaction (Leg 151 Shipboard Scientific Party, 1994; Myhre, Thiede, Firth, et al., 1995). The timing and cause of the overconsolidated section has important implications for Svalbard/Barents Sea ice sheet history. In this contribution, oxygen isotopic stratigraphy in Hole 910A is used to date the termination of overconsolidation near the stage 17/16 boundary at ~670 ka, suggesting a major change in Svalbard/Barents Sea ice sheet history at this time.

METHODS

Samples were dried and weighed, with a small subsample archived for additional work. Samples were then washed over a 63-µm sieve with deionized water only, then dried and weighed again. The >250-µm fraction was also weighed. Individual planktonic foraminifers were handpicked from the >150-µm to <250-µm size fraction for isotopic analysis. The species used throughout the sequence was *N. pachyderma* (sinistrally coiling).

Approximately 20 specimens for isotopic analysis were sonicated in methanol to remove adhering particles, roasted under vacuum at 375°C to oxidize organic contaminants, and reacted in orthophosphoric acid at 90°C. The evolved CO_2 gas was then analyzed on-line using an isotope ratio mass spectrometer. Analyses were made either at the University of California, Santa Barbara, in the laboratory of James Kennett or in the laboratory of Christina Ravelo and James Zachos at the University of California, Santa Cruz. Measurements at UC Santa Barbara were made using a Finnigan/MAT 251 isotope ratio mass spectrometer equipped with an Autoprep Systems carbonate preparation device; those at UC Santa Cruz were made using a Fisons Prism isotope ratio mass spectrometer equipped with an automated preparation device.

Laboratory precision, which was run daily and was based on NBS-20 standards (−4.14‰ for $\delta^{18}O$, −1.06‰ for $\delta^{13}C$) at UC Santa Barbara and on NBS-19 standards (−1.85‰ for $\delta^{18}O$, 2.03‰ for $\delta^{13}C$) at UC Santa Cruz, is 0.1‰ or better. No significant interlaboratory offsets were found, based on analyses of the NBS-19 and −20 standards. Replicate analyses on approximately 20% of the samples demonstrated a reproducibility of ±0.14‰ and ±0.12‰ (mean standard deviation) for $\delta^{18}O$ and $\delta^{13}C$, respectively. No corrections were applied for offsets from isotopic equilibrium in *N. pachyderma* (s) for either $\delta^{18}O$ or $\delta^{13}C$. All isotopic data are expressed using standard δ notation in per mil relative to the Peedee belemnite (PDB) carbonate standard.

RESULTS

Oxygen isotopic data based on *N. pachyderma* (s) (Table 1) from 0 to 15 mbsf exhibit a series of ~1‰ cycles, with values generally ranging from ~3.2‰ to 4.2‰ (Fig. 2). The mean $\delta^{18}O$ values from 15 to 24.5 mbsf are ~0.3‰ lower, and generally range from ~2.9‰ to 3.8‰. Numerous low-$\delta^{18}O$ events occur from 19.8 to 23.7 mbsf.

The carbon isotopic data from 0 to 19.5 mbsf generally range from −0.2‰ to −0.5‰, except for several spikes of ~0.5‰ at 0.06, 1.1, 4.2, 7.9, 9.6, 16.33 and 16.9 mbsf (Fig. 2). Also, the $\delta^{13}C$ values for the top 50 cm are from −0.1 to +0.4‰, significantly higher than the entire lower section. The $\delta^{13}C$ values from 19.5 to 24.5 mbsf exhibit large variations of over 1‰ (ranging from about −0.5‰ to −1.8‰) followed by a large permanent increase of ~1.3‰ centered at ~19.5 mbsf. The $\delta^{13}C$ increase at ~19.5 mbsf coincides with the termination of the overconsolidated section.

The percentage sand fraction (wt% >63 µm) and percentage very coarse sand (wt% >250 µm) remain relatively constant throughout the sequence (~20% and ~3%, respectively; Table 2). Notable exceptions are in the top ~50 cm, at 22.0 and 23.8 mbsf.

DISCUSSION

Stable isotopic data based on *N. pachyderma* (s) provide an isotopic stratigraphy for Hole 910A. Almost 100% core recovery allows generation of nearly continuous isotopic records. The oxygen isotopic data largely reflect the well-known variations in global ice volume during late Quaternary glacial-interglacial cycles (e.g., Shackleton and Opdyke, 1973; Imbrie et al., 1984). Thus, oxygen isotopic stratigraphy provides age control for the sequence, including the top of the overconsolidated section.

Age Control

The oxygen isotopic data clearly show isotope Stages 1 through 16 (and possibly 17), including numerous substages (Fig. 2). For example, three $\delta^{18}O$ minima are seen during Stage 5, which are inferred to correspond to isotope Stages 5a, -c, and -e. Many of the isotope stages are readily assigned (e.g., Stages 1–5, 11, and 15). Also, the stage 12/11 transition stands out as a large, rapid decrease in $\delta^{18}O$, which distinguishes it among late Quaternary deglaciations (Shackleton and Opdyke, 1973; Imbrie et al., 1984). Interpretation of the isotope stratigraphy is aided by the last occurrence (LO) of *Pseudoemiliania lacunosa* at ~9.7 ± 0.75 mbsf (Sato and Kameo, this volume), which is independently dated at 408 ka in Stage 12 (Thierstein et al., 1977; Niitsuma et al., 1991).

An age vs. depth plot showing selected oxygen isotope stage boundaries (ages from Imbrie et al., 1984; Shackleton et al., 1990) and the *P. lacunosa* LO datum is shown in Figure 3. These stratigraphic datums allow calculation of ages and sedimentation rates for the section. Sedimentation rates average ~1.9 cm/k.y. for the 0–245 ka interval and ~3.3 cm/k.y. for the 245–620 ka interval.

The age of the section below ~19 mbsf is more problematic, as the oxygen isotope stratigraphy is more ambiguous. Normal magnetic polarity for the entire sequence suggests an age within the Brunhes Epoch. The problem is that extrapolating the sedimentation rate for the 245–620 ka interval would place the Brunhes/Matuyama boundary at ~22.3 mbsf, but no reversed polarity sediments were recovered. The most likely explanation is that sedimentation rates were higher below ~19 mbsf; rates of at least 4.5 cm/k.y would be required to place the Brunhes/Matuyama boundary at or below 24.2 mbsf.

An alternative interpretation calls for at least one hiatus between 19 and 24.5 mbsf, such that the normal polarity interval from ~19.5 to 24.5 mbsf would represent the lower Brunhes and the Jaramillo Chrons, with much of the upper Matuyama missing (~780–990 ka). Normal polarity sediments in this interval are not assignable to the Olduvai Chron (1.77–1.95 Ma), based on calcareous nannofossil biostratigraphy (Sato and Kameo, this volume). In this view, the ~0.3‰ lower $\delta^{18}O$ values from ~19 to 24.5 mbsf might reflect the well-known lower mean $\delta^{18}O$ values of the middle Quaternary prior to Stage 22 (~900 ka).

However, this alternative requires unreasonable changes in sedimentation rates, particularly during the short Jaramillo Chron (0.99–

Table 1. Stable isotopic data from Hole 910A.

Core, section, interval (cm)	Depth (mbsf)	Age (ka)	$\delta^{18}O$ (‰ PDB)	$\delta^{13}C$ (‰ PDB)
151-910A-				
1H-1, 6–8[a]	0.06	5.54	3.18	0.41
1H-1, 20–22[a]	0.20	14.70	4.25	–0.01
1H-1, 20–22	0.20	14.70	3.95	–0.13
1H-1, 30–32	0.30	18.55	4.22	–0.07
1H-1, 50–52	0.50	26.25	4.18	–0.04
1H-1, 80–82[a]	0.80	37.81	3.90	–0.47
1H-1, 90–92	0.90	41.66	4.17	–0.21
1H-1, 100–102[a]	1.00	45.52	4.03	–0.12
1H-1, 110–112	1.10	49.37	3.46	–0.67
1H-1, 120–122[a]	1.20	53.22	3.64	–0.42
1H-1, 130–132	1.30	57.07	3.56	–0.33
1H-1, 140–142[a]	1.40	60.82	3.93	–0.26
1H-2, 10–12	1.60	68.08	4.01	–0.14
1H-2, 20–22[a]	1.70	71.71	3.75	–0.26
1H-2, 30–32	1.80	75.34	4.00	–0.15
1H-2, 40–42[a]	1.90	78.97	3.58	–0.28
1H-2, 40–42	1.90	78.97	3.88	–0.36
1H-2, 50–52	2.00	82.61	4.04	–0.23
1H-2, 60–62[a]	2.10	86.24	3.96	–0.31
1H-2, 70–72	2.20	89.87	3.86	–0.18
1H-2, 80–82[a]	2.30	93.50	3.23	–0.46
1H-2, 80–82	2.30	93.50	3.71	–0.51
1H-2, 90–92	2.40	97.13	4.00	–0.32
1H-2, 100–102[a]	2.50	100.76	3.64	–0.05
1H-2, 110–112	2.60	104.39	3.93	–0.16
1H-2, 120–122[a]	2.70	108.03	3.59	–0.33
1H-2, 120–122	2.70	108.03	3.81	–0.39
1H-2, 130–132	2.80	111.66	3.71	–0.14
1H-2, 140–142[a]	2.90	115.29	3.28	–0.55
1H-3, 10–12	3.10	122.55	3.95	–0.36
1H-3, 20–22[a]	3.20	126.18	3.37	–0.49
1H-3, 20–22	3.20	126.18	2.97	–0.61
1H-3, 30–32	3.30	132.33	4.06	–0.27
1H-3, 40–42[a]	3.40	141.00	3.71	–0.41
1H-3, 40–42[a]	3.40	141.00	3.75	–0.23
1H-3, 50–52	3.50	149.67	3.78	–0.25
1H-3, 60–62[a]	3.60	158.33	3.77	–0.29
1H-3, 70–72	3.70	167.00	3.88	–0.39
1H-3, 80–82[a]	3.80	175.67	3.63	–0.30
1H-3, 90–92	3.90	184.33	3.80	–0.33
1H-3, 100–102[a]	4.00	193.00	3.81	–0.33
1H-3, 110–112	4.10	201.67	3.46	–0.60
1H-3, 120–122[a]	4.20	210.33	2.96	–1.31
1H-3, 120–122	4.20	210.33	3.39	–0.43
1H-3, 130–132	4.30	219.00	3.95	–0.29
1H-3, 140–142[a]	4.40	227.67	3.78	–0.33
1H-4, 10–12	4.60	245.00	3.88	–0.38
1H-4, 20–22[a]	4.70	248.42	4.12	–0.25
1H-4, 30–32	4.80	251.84	4.03	–0.23
1H-4, 40–42[a]	4.90	255.25	3.75	–0.36
1H-4, 50–52	5.00	258.67	3.83	–0.32
1H-4, 60–62[a]	5.10	262.09	3.83	–0.34
1H-4, 70–72	5.30	268.93	3.95	–0.22
1H-CC, 10–12	5.36	270.98	3.97	–0.47
1H-CC, 18–20	5.44	273.71	3.74	–0.39
2H-1, 10–12	5.60	279.18	3.90	–0.37
2H-1, 23–25[a]	5.73	283.63	3.76	–0.32
2H-1, 30–32	5.80	286.02	3.98	–0.37
2H-1, 40–42	5.90	289.44	4.04	–0.22
2H-1, 50–52	6.00	292.85	4.11	–0.29
2H-1, 60–62[a]	6.10	296.27	3.24	–0.49
2H-1, 60–62	6.10	296.27	3.47	–0.25
2H-1, 70–72	6.20	299.69	3.92	–0.32
2H-1, 80–82[a]	6.30	303.11	3.88	–0.31
2H-1, 90–92	6.40	306.53	3.65	–0.23
2H-1, 100–102[a]	6.50	309.95	3.06	–0.40
2H-1, 100–102[a]	6.50	309.95	3.66	–0.41
2H-1, 110–112	6.60	313.36	3.49	–0.51
2H-1, 120–122	6.70	316.78	4.04	–0.35
2H-1, 120–122	6.70	316.78	3.88	–0.46
2H-1, 140–142[a]	6.90	323.62	3.42	–0.30
2H-2, 10–12	7.10	330.45	3.68	–0.35
2H-2, 23–35[a]	7.23	334.90	3.82	–0.28
2H-2, 30–32	7.30	337.29	3.50	–0.39
2H-2, 40–42[a]	7.40	340.65	4.09	–0.27
2H-2, 50–52	7.50	343.94	3.98	–0.36
2H-2, 60–62[a]	7.60	347.24	3.63	–0.35
2H-2, 70–72	7.70	350.53	3.54	–0.20
2H-2, 80–82	7.80	353.82	3.73	–0.36
2H-2, 90–92	7.90	357.12	3.55	–1.11
2H-2, 90–92	7.90	357.12	4.00	–3.12
2H-2, 100–102[a]	8.00	360.41	3.66	–0.30
2H-2, 110–112	8.10	363.71	3.57	–0.41
2H-2, 120–122	8.20	367.00	3.94	–0.32
2H-2, 130–132	8.30	370.29	3.88	–0.28
2H-2, 140–142[a]	8.40	373.59	3.95	–0.37
2H-3, 10–12	8.60	380.18	3.64	–0.19
2H-3, 23–25[a]	8.73	384.46	3.85	–0.52
2H-3, 30–32	8.80	386.76	3.59	–0.56
2H-3, 40–42[a]	8.90	390.06	3.67	–0.46
2H-3, 40–42[a]	8.90	390.06	3.81	–0.36
2H-3, 50–52	9.00	393.35	3.80	–0.46
2H-3, 60–62[a]	9.10	396.65	3.47	–0.52
2H-3, 70–72	9.20	399.94	3.55	–0.34
2H-3, 83–85	9.33	404.22	3.63	–0.50
2H-3, 90–92	9.40	406.53	3.41	–0.79
2H-3, 100–102[a]	9.50	409.82	3.10	–1.02
2H-3, 100–102	9.50	409.82	3.42	–1.54
2H-3, 110–112	9.60	413.12	3.03	–1.36
2H-3, 120–122	9.70	416.41	3.71	–0.55
2H-3, 130–132	9.80	419.71	3.73	–0.41
2H-3, 140–142[a]	9.90	423.00	3.83	–0.47
2H-4, 10–12	10.10	427.81	3.82	–0.47
2H-4, 23–25[a]	10.23	430.94	3.92	–0.44
2H-4, 30–32	10.30	432.62	3.96	–0.43
2H-4, 40–42[a]	10.40	435.02	4.15	–0.35
2H-4, 50–52	10.50	437.43	3.41	–0.46
2H-4, 50–52	10.50	437.43	3.42	–0.92
2H-4, 60–62[a]	10.60	439.83	3.76	–0.59
2H-4, 70–72	10.70	442.24	3.80	–0.55
2H-4, 82–84	10.82	445.12	4.01	–0.41
2H-4, 90–92	10.90	447.05	3.83	–0.47
2H-4, 100–102[a]	11.00	449.45	3.64	–0.43
2H-4, 110–112	11.10	451.86	3.75	–0.39
2H-4, 120–122	11.20	454.26	3.87	–0.51
2H-4, 130–132	11.30	456.67	3.55	–0.39
2H-5, 10–12	11.60	463.88	3.49	–0.41
2H-5, 23–25[a]	11.73	467.01	3.84	–0.33
2H-5, 30–32	11.80	468.69	3.70	–0.50
2H-5, 40–42	11.90	471.10	4.06	–0.38
2H-5, 50–52	12.00	473.50	3.71	–0.46
2H-5, 60–62[a]	12.10	475.90	3.31	–0.23
2H-5, 60–62	12.10	475.90	3.85	–0.47
2H-5, 70–72	12.20	478.31	3.15	–0.77
2H-5, 80–82	12.30	480.71	3.94	–0.38
2H-5, 80–82	12.30	480.71	3.76	–0.48
2H-5, 90–92	12.40	483.12	3.56	–0.56
2H-5, 100–102[a]	12.50	485.52	3.76	–0.55
2H-5, 110–112	12.60	487.93	3.58	–0.40
2H-5, 120–122	12.70	490.33	3.62	–0.36
2H-5, 130–132	12.80	492.74	3.52	–0.51
2H-5, 140–142[a]	12.90	495.14	3.93	–0.36
2H-6, 10–12	13.10	499.95	3.58	–0.55
2H-6, 23–25	13.23	503.08	4.02	–0.36
2H-6, 23–25	13.23	503.08	3.94	–0.46
2H-6, 30–32	13.30	504.76	3.53	–0.44
2H-6, 40–42[a]	13.40	507.17	3.38	–0.48
2H-6, 50–52	13.50	509.57	3.75	–0.31
2H-6, 60–62[a]	13.60	511.98	3.71	–0.20
2H-6, 70–72	13.70	514.38	3.25	–0.33
2H-6, 80–82	13.80	516.79	3.56	–0.19
2H-6, 100–102[a]	14.00	521.60	3.45	–0.42
2H-CC, 10–12	14.20	527.15	3.86	–0.33
2H-CC, 23–25[a]	14.32	530.92	3.71	–0.43
2H-CC, 30–32	14.40	533.44	3.91	–0.47
3H-1, 10–12	15.10	555.48	3.99	–0.38
3H-1, 20–22[a]	15.20	558.62	3.79	–0.44
3H-1, 20–22[a]	15.20	558.62	3.18	–0.48
3H-1, 30–32	15.30	561.77	3.63	–0.45
3H-1, 40–42	15.40	564.92	3.77	–0.36
3H-1, 50–52	15.50	568.07	3.09	–0.46
3H-1, 60–62[a]	15.60	571.21	3.26	–0.51
3H-1, 70–72	15.70	574.36	3.30	–0.56
3H-1, 81–83	15.81	577.82	3.54	–0.46
3H-1, 90–92	15.90	580.66	3.67	–0.59
3H-1, 100–102[a]	16.00	583.80	3.60	–0.45
3H-1, 110–112	16.10	586.95	3.74	–0.30
3H-1, 120–122	16.20	590.10	3.71	–0.30
3H-1, 133–135	16.33	594.19	3.30	–1.21
3H-1, 133–135	16.33	594.19	3.16	–0.80
3H-1, 140–142[a]	16.40	596.39	3.13	–0.66
3H-2, 30–32	16.80	608.98	3.88	–0.36
3H-2, 30–32	16.80	608.98	3.03	–1.96
3H-2, 40–42[a]	16.90	612.13	2.73	–1.21
3H-2, 40–42	16.90	612.13	3.14	–0.72
3H-2, 40–42	16.90	612.13	3.50	–1.31
3H-2, 50–52	17.00	615.28	2.99	–0.60
3H-2, 60–62[a]	17.10	618.43	3.26	–0.54
3H-2, 60–62	17.10	618.43	3.59	–0.48
3H-2, 70–72	17.20	621.14	3.41	–0.29
3H-2, 81–83	17.31	623.66	3.56	–0.37
3H-2, 90–92	17.40	625.72	3.73	–0.51
3H-2, 100–102[a]	17.50	672.8	3.51	–0.48
3H-2, 100–102[a]	17.50	628.01	3.24	–0.53
3H-2, 110–112	17.60	630.30	3.50	–0.46

Table 1 (continued).

Core, section, interval (cm)	Depth (mbsf)	Age (ka)	$\delta^{18}O$ (‰ PDB)	$\delta^{13}C$ (‰ PDB)
3H-2, 120–122	17.70	632.58	3.49	–0.45
3H-2, 130–132	17.80	634.87	3.40	–0.53
3H-2, 140–142[a]	17.90	637.16	3.24	–0.53
3H-2, 140–142	17.90	637.16	3.62	–0.50
3H-3, 10–12	18.10	641.74	3.39	–0.38
3H-3, 20–22	18.20	644.02	3.59	–0.73
3H-3, 30–32	18.30	646.31	3.78	–0.42
3H-3, 40–42[a]	18.40	648.60	3.56	–0.42
3H-3, 48–58	18.48	650.43	3.77	–0.58
3H-3, 60–62	18.60	653.18	3.36	–0.70
3H-3, 70–72	18.70	655.46	3.58	–0.55
3H-3, 80–82	18.80	657.75	3.68	–0.65
3H-3, 90–92	18.90	660.04	3.71	–0.35
4H-1, 10–12	19.60	676.06	3.10	–1.14
4H-1, 20–22[a]	19.70	678.34	3.05	–0.91
4H-1, 30–32	19.80	680.63	2.90	–1.09
4H-1, 40–42	19.90	682.92	3.38	–1.03
4H-1, 50–52	20.00	685.21	3.64	–0.86
4H-1, 60–62[a]	20.10	687.50	3.04	–1.26
4H-1, 70–72	20.20	689.78	2.94	–1.69
4H-1, 80–82	20.30	692.07	2.98	–1.15
4H-1, 90–92	20.40	694.36	3.44	–1.27
4H-1, 100–102[a]	20.50	696.65	3.22	–1.07
4H-1, 110–112	20.60	698.94	3.73	–0.93
4H-1, 110–112	20.60	698.94	3.75	–0.46
4H-1, 120–122	20.70	701.22	3.27	–1.41
4H-1, 130–132	20.80	703.51	3.40	–1.22
4H-1, 140–142[a]	20.90	705.80	2.97	–1.84
4H-1, 140–142	20.90	705.80	4.04	–0.17
4H-2, 10–12	21.10	710.38	3.30	–0.96
4H-2, 18–20[a]	21.18	712.21	3.00	–0.90
4H-2, 30–32	21.30	714.95	3.62	–0.68
4H-2, 40–42[a]	21.40	717.24	3.42	–0.88
4H-2, 50–52	21.50	719.53	3.57	–0.91
4H-2, 60–62[a]	21.60	721.82	3.37	–0.63
4H-2, 70–72	21.70	724.10	3.71	–0.66
4H-2, 80–82[a]	21.80	726.39	3.76	–0.65
4H-2, 90–92	21.90	728.68	3.04	–0.53
4H-2, 110–112	22.10	733.26	4.52	–0.40
4H-2, 110–112	22.10	733.26	4.11	–1.55
4H-2, 120–122	22.20	735.54	3.30	–1.20
4H-2, 130–132	22.30	737.83	3.16	–1.77
4H-2, 138–140	22.38	739.66	3.24	–1.43
4H-3, 10–12	22.60	744.70	3.65	–1.32
4H-3, 20–22[a]	22.70	746.98	2.79	–1.31
4H-3, 20–22	22.70	746.98	3.22	–0.99
4H-3, 30–32	22.80	749.27	3.16	–1.32
4H-3, 40–42	22.90	751.56	3.54	–1.40
4H-3, 50–52	23.00	753.85	3.51	–1.31
4H-3, 60–62[a]	23.10	756.14	3.08	–1.13
4H-3, 70–72	23.20	758.42	3.38	–1.21
4H-3, 80–82	23.30	760.71	3.19	–1.45
4H-3, 90–92	23.40	763.00	3.40	–1.16
4H-3, 100–102[a]	23.50	765.29	3.74	–0.40
4H-3, 110–112	23.60	767.58	3.17	–1.32
4H-3, 120–122	23.70	769.86	2.64	–1.08
4H-3, 120–122	23.70	769.86	3.24	–1.38
4H-4, 10–12	24.10	779.02	3.10	–1.03
4H-4, 20–22[a]	24.20	781.78	3.68	–0.71
4H-4, 20–22	24.20	781.78	3.90	–0.41

Note: [a]Sample analyzed at the University of California, Santa Barbara. All other samples analyzed at the University of California, Santa Cruz.

1.07 Ma). Further, interpolation between the 15/16 stage boundary and the first occurrence (FO) of *Gephyrocapsa oceanica* (1.70 Ma; Raffi et al., 1993) between Sections 151-910C-7R-CC and 8R-CC (Sato and Kameo, this volume) yields a minimum estimate of ~4.0 cm/k.y. for the 17–60 mbsf interval. Based on this evidence for higher average sedimentation rates in this interval, I concur with the assignment of Hole 910A to the Brunhes Chron (Shipboard Scientific Party, 1995) and conclude that no major hiatus exists in the upper 24.5 m in Hole 910A and assign ages for the 19–24.5 mbsf section accordingly. As an aside, a hiatus that removed much of the lower Quaternary to upper Pliocene is found at the base of the overconsolidated section between ~70 and 95 mbsf, based on biostratigraphy (Site 910; Myhre, Thiede, Firth, et al., 1995). These interpretations await independent assessment of ages within the overconsolidated section, such as strontium isotopic stratigraphy.

Thus, oxygen isotopic stratigraphy in the overlying sequence dates the top of the overconsolidated section near the Stage 17/16 boundary (~670 ka).

Carbon Isotopic Record

The carbon isotopic record is remarkably stable during the interval from ~620 ka to the present, with the exception of large spikes of ~0.5‰ mainly during inferred interglacials (Fig. 4). Also, the top 20 cm features the highest $\delta^{13}C$ values observed in the core (–0.1‰ to 0.4‰), suggesting a fundamentally different hydrography in the Holocene. The major features of the $\delta^{13}C$ record, however, are two large-amplitude cycles of ~1‰ within the overconsolidated section. A 1.3‰ increase coincides with the top of this section. Thus, the overconsolidated section is marked by a fundamentally different $\delta^{13}C$ signal than the upper Quaternary section. Such large $\delta^{13}C$ fluctuations are unknown in middle Quaternary global $\delta^{13}C$ records (e.g., Shackleton and Hall, 1989; Berger et al., 1993). However, lower magnitude fluctuations are present in middle to late Quaternary benthic $\delta^{13}C$ records from the North Atlantic (e.g., Ruddiman et al., 1989). The magnitude of Hole 910A $\delta^{13}C$ cycles suggests highly variable conditions specific to the Yermak Plateau region prior to ~620 ka. These $\delta^{13}C$ fluctuations do not seem to correlate with any measured parameter of the Hole 910A sequence, including sedimentological parameters such as grain size, density, or porosity. Nevertheless, the ~1‰ $\delta^{13}C$ fluctuations prior to ~620 ka may well be genetically linked to the same processes that resulted in an overconsolidated section below ~19 mbsf.

Assuming that *N. pachyderma* (s) reflects surface water $\delta^{13}C$ values, the ~1‰ variations prior to ~620 ka may reflect large changes in the $\delta^{13}C$ of ΣCO_2 over the Yermak Plateau. This assumption is based on recent findings that *N. pachyderma* (s) accurately records mixed layer $\delta^{13}C$ in the Greenland Sea (Kohfeld et al., 1994; Johannessen et al., in press). Such changes might be produced either by variations in organic matter concentrations or by changes in "thermodynamic tagging" of surface water ΣCO_2 by air-sea exchange (Charles and Fairbanks, 1990). Thermodynamic tagging should increase surface water $\delta^{13}C$ (Charles and Fairbanks, 1990). However, modern surface waters at 80°N show significant thermodynamic depletion (Charles et al., 1993), yet Holocene $\delta^{13}C$ values are the highest of the late Quaternary in Hole 910A. As the $\delta^{13}C$ values within the overconsolidated section are anomalously low relative to modern values, the potential control by thermodynamic gas exchange seems unlikely.

Alternatively, large-scale changes in upwelling may explain the large 1‰ $\delta^{13}C$ variations prior to ~620 ka, as also observed in the central Arctic during the last deglaciation (Stein et al., 1994). Or, input of terrestrially derived organic carbon (with lower $\delta^{13}C$ values) may have been greater, due to more dynamic glacial processes. In short, these large $\delta^{13}C$ variations still require explanation, and the question is open as to how they relate to the processes of overconsolidation.

Interpretations of the Overconsolidated Section

Interpretations of the overconsolidated section include (1) episodic grounding of a marine-based ice sheet, perhaps derived from the Barents Sea ice sheet and buttressed by Svalbard, which overcompacted the sediments on the Yermak Plateau, and/or (2) coarser-grained glacial sedimentation that allowed enhanced compaction during this interval (Myhre, Thiede, Firth, et al., 1995; Rack et al., Chapter 21, this volume). Overcompaction may have also resulted from large icebergs grounding at an inferred water depth of at least 400 m. Grounding of recent icebergs on the Yermak Plateau at water depths of ~450 to 850 m has been demonstrated based on sidescan sonar and 3.5-kHz profiling, although the age is not well known (Vogt et al., 1994). Also, the Yermak Plateau exhibits a beveled surface, which may indicate the presence of grounded ice during the late Quaternary (Vogt et al., 1994, 1995). In areas of ice sheet or iceberg grounding, large-scale erosion under the ice and redeposition are common (e.g., Vorren et al., 1988). A major hiatus indeed exists at the base of the

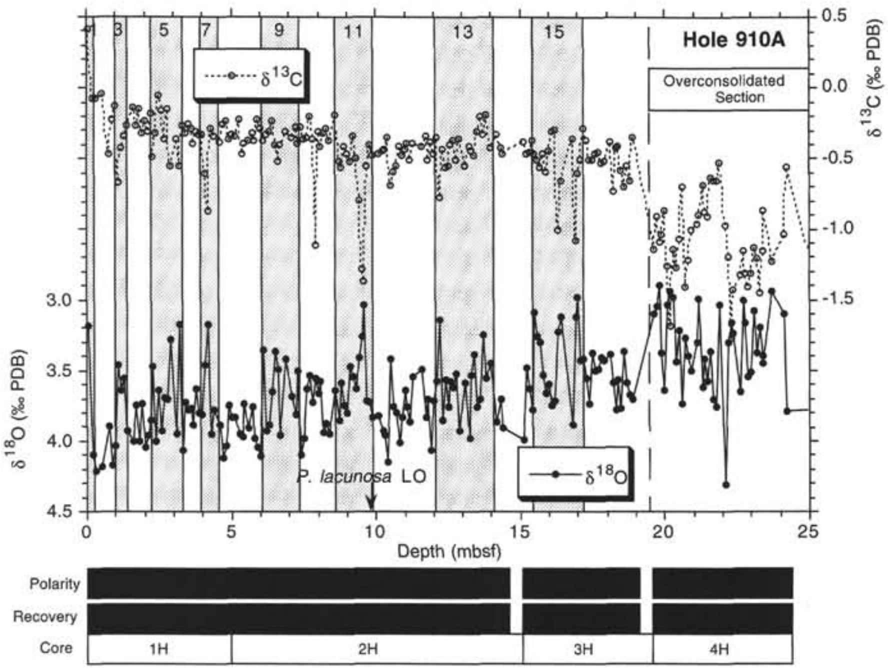

Figure 2. Hole 910A $\delta^{18}O$ and $\delta^{13}C$ data vs. depth, based on *N. pachyderma* (sinistrally coiling). Oxygen isotope Stages 1 through 16 are present in the upper 19 mbsf. The LO of *P. lacunosa* is at 9.7 ± 0.75 mbsf. The overconsolidated section below ~19.5 mbsf is marked by large (>1‰) shifts in $\delta^{13}C$. Core recovery and normal magnetic polarity are shown in black.

overconsolidated section between ~70 and 95 mbsf, but there is no evidence for a hiatus near the top at ~19.5 mbsf.

Alternatively, overcompaction may have resulted from coarser grained sedimentation, because sandy clays are more easily compacted than silty clays (Hamilton, 1976). There is some evidence for more numerous particles >2 mm in diameter from ~16 to 25 mbsf, based on X-ray imaging of Hole 910D cores (Rack et al., Chapter 21, this volume). However, coarse grain size data show no mean differences in grain size (>63- and >250-µm fractions) in the overconsolidated section (Fig. 5), arguing against this hypothesis. Geotechnical and geomagnetic investigations are being conducted to further differentiate possible causes of overcompaction (Rack et al., Chapter 21, this volume; Solheim et al., unpubl. data; Williamson et al., unpubl. data).

Quaternary Arctic Gateway Paleoceanography

In addition to age control, stable isotopic data from Hole 910A provide records of late Quaternary surface water environments in the Yermak Plateau region of the Arctic Ocean. The series of ~1‰ $\delta^{18}O$ cycles from 0 to 670 ka are inferred to largely reflect the well-known variations in Quaternary ice volumes, although the record is complicated by minor salinity variations (Fig. 6). Salinity variations are significantly less than in the Arctic Ocean (e.g., Morris, 1988). Interestingly, the Hole 910A $\delta^{18}O$ amplitude is ~0.2‰ to 0.4‰ lower than the generally accepted 1.2‰–1.4‰ attributed to Quaternary ice-growth and decay (e.g., Shackleton and Opdyke, 1973; Fairbanks and Matthews, 1978; Mix and Ruddiman, 1984; Fairbanks, 1989), although this may reflect minor undersampling of glacial/interglacial values. With this caveat, salinity effects appear to have been relatively minor, as the $\delta^{18}O$ amplitude is not increased beyond the ice volume effect of ~1.2‰ to 1.4‰.

Possible explanations for dampened glacial-interglacial $\delta^{18}O$ amplitudes on the Yermak Plateau relate to the regional oceanography. Surface water $\delta^{18}O$ in this region is very sensitive to salinity differences (e.g., Fairbanks et al., 1992). The warm, high salinity WSC has a distinctly higher $\delta^{18}O$ signature than the low salinity East Greenland Current (EGC) (by up to 1.5‰; Johannessen et al., in press). A higher influx of WSC waters during interglacials and a higher outflow of EGC waters during glacials would significantly dampen the glacial-interglacial $\delta^{18}O$ amplitude. Alternatively, changes in the seasonal and/or depth preferences of *N. pachyderma* (s) may have resulted in dampened $\delta^{18}O$ amplitudes.

In contrast to the last 670 k.y., $\delta^{18}O$ values prior to ~670 ka are ~0.3‰ lower, whereas maintaining a similar range of ~1‰. This ~0.3‰ difference is probably not attributable to lower global ice volumes of the middle Quaternary, based on the age control discussed above. Instead, the ~0.3‰ difference may reflect a different temperature and/or salinity regime in the early Brunhes Chron. However, there is little evidence for warmer surface waters in the Norwegian Sea, which might have been advected into the Arctic Ocean via the West Spitsbergen Current and the Barents Sea branch. Indeed, the warmest temperatures in the Norwegian Sea are indicated for the entirety of the last 1 m.y., based on planktonic foraminifer flux records and percentage carbonate records inferred to reflect temperature-dependent carbonate production (Jansen et al., 1988; Spiegler and Jansen, 1989; Henrich, 1989). Thus the ~0.3‰ difference observed prior to 670 ka may represent slightly lower mean salinities for Yermak Plateau surface waters (by ~0.3‰, based on the calibration of Fairbanks et al., 1992).

Lower mean salinities might be due to (1) higher meltwater input and/or (2) a different glacial meltwater source marked by lower $\delta^{18}O$. If the meltwater input were higher, the interval prior to ~670 ka might reflect greater instability in the circum-Arctic ice sheets. One would think, however, that the amplitude of the $\delta^{18}O$ variations would be larger if such a mechanism were operating, but it was ~1‰ both before and after 670 ka. Stated another way, both the glacial maxima and the interglacial minima are offset by ~0.3‰, instead of preferential decreases during interglacials that might suggest stronger meltwater effects. Alternatively, surface water $\delta^{18}O$ may have been influenced by a lower-$\delta^{18}O$ glacial meltwater source. The $\delta^{18}O$ of modern glacial ice masses in the Northern Hemisphere ranges from ~−10‰ to −30‰, dependent upon the moisture source and the altitude of deposition (e.g., Dansgaard et al., 1973). Thus, the ~0.5‰ lower $\delta^{18}O$ surface water values might reflect a different source, such as the larger Greenland ice sheet instead of the smaller Svalbard dome.

Relation to the Middle Quaternary Transition

The cause of the middle Quaternary climatic transition (from climates dominated by ~41 k.y. periodicity to ~100 k.y. periodicity,

Table 2. Size fraction data from Hole 910A.

Core, section, interval (cm)	Depth (mbsf)	Age (ka)	Dry weight (g)	>63-µm weight (g)	>250-µm weight (g)
151-910A-					
1H-1, 10–12	0.10	9.23	12.7900	2.6933	0.8624
1H-1, 20–22	0.20	14.70	13.5214	6.5308	3.6793
1H-1, 30–32	0.30	18.55	8.8190	2.9000	0.8623
1H-1, 40–42	0.40	22.40	18.2146	4.6014	0.5229
1H-1, 50–52	0.50	26.259	9.0720	4.6590	1.3875
1H-1, 60–62	0.60	30.11	17.6799	11.4118	4.4616
1H-1, 70–72	0.70	33.96	10.3050	2.3031	0.7382
1H-1, 80–82	0.80	37.81	13.5770	2.7025	0.3359
1H-1, 90–92	0.90	41.66	12.0370	2.2043	0.3447
1H-1, 100–102	1.00	45.52	17.1058	3.6106	0.4480
1H-1, 110–112	1.10	49.37	11.2560	1.9127	0.2342
1H-1, 120–122	1.20	53.22	13.8451	2.6222	0.3799
1H-1, 130–132	1.30	57.07	13.4280	2.2468	0.3318
1H-1, 140–142	1.40	60.82	14.2409	2.9141	0.4497
1H-2, 10–12	1.60	68.08	10.6360	1.6720	0.2178
1H-2, 20–22	1.70	71.71	13.9723	2.6230	0.3410
1H-2, 30–32	1.80	75.34	15.2380	2.9195	0.7258
1H-2, 40–42	1.90	78.97	14.1832	2.6779	0.3735
1H-2, 50–52	2.00	82.61	12.9760	1.9912	0.3290
1H-2, 60–62	2.10	86.24	15.9170	3.0524	0.4975
1H-2, 70–72	2.20	89.87	15.4450	2.6566	0.3973
1H-2, 80–82	2.30	93.50	14.4154	2.5932	0.3178
1H-2, 90–92	2.40	97.13	12.9690	2.2477	0.3800
1H-2, 100–102	2.50	100.76	17.5947	3.4031	0.4555
1H-2, 110–112	2.60	104.39	11.7160	1.9300	0.2190
1H-2, 120–122	2.70	108.03	14.4115	2.8332	0.4299
1H-2, 130–132	2.80	111.66	10.6940	2.0075	0.4468
1H-2, 140–142	2.90	115.29	15.6597	2.8086	0.3746
1H-3, 10–12	3.10	122.55	17.3810	3.3904	0.6348
1H-3, 20–22	3.20	126.18	16.9628	3.5216	0.6273
1H-3, 30–32	3.30	132.33	13.7360	2.4487	0.4494
1H-3, 40–42	3.40	141.00	16.9232	3.2938	0.3989
1H-3, 50–52	3.50	149.67	13.4950	2.2338	0.2908
1H-3, 60–62	3.60	158.33	16.0059	3.1865	0.4730
1H-3, 70–72	3.70	167.00	16.9760	2.7932	0.4625
1H-3, 80–82	3.80	175.67	19.4209	4.2777	1.0940
1H-3, 90–92	3.90	184.33	14.0510	2.3665	0.3319
1H-3, 100–102	4.00	193.00	18.5700	2.2843	0.2981
1H-3, 110–112	4.10	201.67	15.5510	1.9162	0.2762
1H-3, 120–122	4.20	210.33	17.6455	3.4332	0.4261
1H-3, 130–132	4.30	219.00	15.1950	2.7082	0.5681
1H-3, 140–142	4.40	227.67	16.8316	3.3198	0.4429
1H-4, 10–12	4.60	245.00	15.8320	2.7449	0.4496
1H-4, 20–22	4.70	248.42	18.0760	3.5278	0.4403
1H-4, 30–32	4.80	251.84	12.7760	2.3530	0.4418
1H-4, 40–42	4.90	255.25	15.3520	3.0033	0.5285
1H-4, 50–52	5.00	258.67	16.8940	2.5923	0.3510
1H-4, 60–62	5.10	262.09	20.9901	3.6791	0.4733
1H-4, 70–72	5.20	265.51	18.8970	3.0069	0.4008
1H-CC, 10–12	5.36	270.98	17.6240	3.0281	0.5228
1H-CC, 18–20	5.44	273.71	18.8318	3.6484	0.5415
2H-1, 10–12	5.60	279.18	13.3511	2.8532	0.3688
2H-1, 23–25	5.73	283.63	12.0385	2.3424	0.7213
2H-1, 30–32	5.80	286.02	13.1117	2.1198	0.2439
2H-1, 40–42	5.90	289.44	13.1545	2.5491	0.3109
2H-1, 50–52	6.00	292.85	10.9556	2.6172	0.3829
2H-1, 60–62	6.10	296.27	13.5544	2.0656	0.2781
2H-1, 70–72	6.20	299.69	14.2452	2.4450	0.3275
2H-1, 80–82	6.30	303.11	16.7326	3.2607	0.3716
2H-1, 90–92	6.40	306.53	10.4790	1.9739	0.2775
2H-1, 100–102	6.50	309.95	11.0327	2.0922	0.2624
2H-1, 110–112	6.60	313.36	9.4925	2.0373	0.4306
2H-1, 120–122	6.70	316.78	12.9248	2.5800	0.3265
2H-1, 140–142	6.90	323.62	10.8698	2.8374	0.2595
2H-2, 10–12	7.10	330.45	10.7630	2.0037	0.2564
2H-2, 23–25	7.23	334.90	20.1992	3.6509	0.4628
2H-2, 30–32	7.30	337.29	11.7781	2.2484	0.3270
2H-2, 40–42	7.40	340.65	11.5120	2.1117	0.2947
2H-2, 50–52	7.50	343.94	14.6505	2.8913	0.4568
2H-2, 60–62	7.60	347.24	15.8925	2.8898	0.5097
2H-2, 70–72	7.70	350.53	19.0191	3.6726	0.5657
2H-2, 80–82	7.80	353.82	17.3415	3.3273	0.5924
2H-2, 90–92	7.90	357.12	9.0922	1.7866	0.2937
2H-2, 100–102	8.00	360.41	12.4862	2.3585	0.3168
2H-2, 110–112	8.10	363.71	11.8194	2.5555	0.5469
2H-2, 120–122	8.20	367.00	11.3649	2.0820	0.2589
2H-2, 130–132	8.30	370.29	10.5095	2.0838	0.2932
2H-2, 140–142	8.40	373.59	10.4627	2.0764	0.3154
2H-3, 10–12	8.60	380.18	18.6006	4.5537	0.5836
2H-3, 23–25	8.73	384.46	18.1485	3.3268	0.5126
2H-3, 30–32	8.80	386.76	20.3179	3.8810	0.6056
2H-3, 40–42	8.90	390.06	17.5216	3.1812	0.4068
2H-3, 50–52	9.00	393.35	13.9577	2.4016	0.3476
2H-3, 60–62	9.10	396.65	12.2472	2.6074	0.4049
2H-3, 70–72	9.20	399.94	16.0727	3.0481	0.4461
2H-3, 83–85	9.33	404.22	20.6184	4.0212	0.6792
2H-3, 90–92	9.40	406.53	12.3885	1.9880	0.2799
2H-3, 100–102	9.50	409.82	11.4235	2.0021	0.3891
2H-3, 110–112	9.60	413.12	11.4878	1.8971	0.2601
2H-3, 120–122	9.70	416.41	11.3502	1.9667	0.2240
2H-3, 130–132	9.80	419.71	10.3025	2.4619	0.4604
2H-3, 140–142	9.90	423.00	10.7226	2.2113	0.3670
2H-4, 10–12	10.10	427.81	14.7798	3.0929	0.4921
2H-4, 23–25	10.23	430.94	19.1175	3.7135	0.4314
2H-4, 30–32	10.30	432.62	18.8796	3.6512	0.4576
2H-4, 40–42	10.40	435.02	18.4420	3.4779	0.5379
2H-4, 50–52	10.50	437.43	14.1287	1.0237	0.2742
2H-4, 60–62	10.60	439.83	16.1548	3.0182	0.4823
2H-4, 70–72	10.70	442.24	17.5683	3.6749	0.7630
2H-4, 82–84	10.82	445.12	18.5014	3.2072	0.5437
2H-4, 90–92	10.90	447.05	14.4876	4.3603	0.3695
2H-4, 100–102	11.00	449.45	15.0013	2.3864	0.3036
2H-4, 110–112	11.10	451.86	13.4703	2.7952	0.4095
2H-4, 120–122	11.20	454.26	12.0621	2.2490	0.3266
2H-4, 130–132	11.30	456.67	11.8541	2.1013	0.2365
2H-5, 10–12	11.60	463.88	14.7034	2.6990	0.3268
2H-5, 23–25	11.73	467.01	19.0091	2.6925	0.3877
2H-5, 30–32	11.80	468.69	12.3379	2.2665	0.3631
2H-5, 40–42	11.90	471.10	17.2163	3.2005	0.4266
2H-5, 50–52	12.00	473.50	14.5869	3.0541	0.3658
2H-5, 60–62	12.10	475.90	18.2814	3.4597	0.7176
2H-5, 70–72	12.20	478.31	16.4500	3.0478	0.6038
2H-5, 80–82	12.30	480.71	18.1333	4.4874	0.4349
2H-5, 90–92	12.40	483.12	16.8644	3.9640	0.3501
2H-5, 100–102	12.50	485.52	14.0914	2.5520	0.3405
2H-5, 110–112	12.60	487.93	11.9443	2.3218	0.3270
2H-5, 120–122	12.70	490.33	12.2217	2.1225	0.2599
2H-5, 130–132	12.80	492.74	11.9843	2.3124	0.3897
2H-5, 140–142	12.90	495.14	15.3099	2.5444	0.3206
2H-6, 10–12	13.10	499.95	17.0589	3.2332	0.4455
2H-6, 23–25	13.23	503.08	19.3568	3.6201	0.4714
2H-6, 30–32	13.30	504.76	17.5568	3.3223	0.3818
2H-6, 40–42	13.40	507.17	12.4596	2.2861	0.4717
2H-6, 50–52	13.50	509.57	13.7686	2.3645	0.3678
2H-6, 60–62	13.60	511.98	15.9301	2.7154	0.3578
2H-6, 70–72	13.70	514.38	16.6813	2.9613	0.3592
2H-6, 80–82	13.80	516.79	18.1165	3.1957	0.3897
2H-6, 90–92	13.90	519.19	18.7411	3.5996	0.6006
2H-6, 100–102	14.00	521.60	14.5652	2.6504	0.4146
2H-CC, 10–12	14.19	526.83	16.0385	2.9933	0.5850
2H-CC, 23–25	14.32	530.92	18.7895	3.6456	0.7213
2H-CC, 30–32	14.39	533.13	17.7674	3.6464	0.4834
3H-1, 10–12	15.20	558.62	16.0969	3.0718	0.3381
3H-1, 20–22	15.30	561.77	19.1038	3.5788	0.4628
3H-1, 30–31	15.40	564.92	18.0048	3.5136	0.4480
3H-1, 40–42	15.50	568.07	20.1524	3.5613	0.5272
3H-1, 50–52	15.60	571.21	16.8382	3.6013	0.8463
3H-1, 60–62	15.70	574.36	16.7388	2.6882	0.3329
3H-1, 70–72	15.80	577.51	16.0962	3.1101	0.4943
3H-1, 81–83	15.91	580.97	15.9825	1.9396	0.2725
3H-1, 90–92	16.00	583.80	16.5375	3.2024	0.4367
3H-1, 110–112	16.10	586.95	15.5980	2.4891	0.3461
3H-1, 120–122	16.20	590.10	16.6152	2.2373	0.3005
3H-1, 133–135	16.33	594.19	16.2882	2.6858	0.4421
3H-1, 140–142	16.40	596.39	16.3650	2.3235	0.2290
3H-2, 10–12	16.60	602.69	14.7503	2.8273	0.4019
3H-2, 20–22	16.70	605.84	15.0114	2.6998	0.2454
3H-2, 30–32	16.80	608.98	18.5784	3.8044	0.6678
3H-2, 40–42	16.90	612.13	14.5174	3.4340	0.6711
3H-2, 50–52	17.00	615.28	15.8870	3.2898	0.4285
3H-2, 60–62	17.10	618.43	16.2404	2.8793	0.5283
3H-2, 70–72	17.20	621.14	15.6278	3.1323	0.4877
3H-2, 81–83	17.31	623.66	17.2143	3.2684	0.5218
3H-2, 90–92	17.40	625.72	16.6143	3.2562	0.7644
3H-2, 100–102	17.50	628.01	15.8871	2.4038	0.3818
3H-2, 110–112	17.60	630.30	15.1276	2.3816	0.3066
3H-2, 120–122	17.70	632.58	18.1834	3.0412	0.4158
3H-2, 132–134	17.82	635.33	16.2509	2.9376	0.3506
3H-2, 140–142	17.90	637.16	16.9032	2.6422	0.3599
3H-3, 10–12	18.10	641.74	17.9785	3.2932	0.3621
3H-3, 20–22	18.20	644.02	18.8340	3.5380	0.3649
3H-3, 30–32	18.30	646.31	17.1969	3.4531	0.4539
3H-3, 40–42	18.40	648.60	16.5056	3.2136	0.4612
3H-3, 48–50	18.48	650.43	15.7488	3.2647	0.4580
3H-3, 60–62	18.60	653.18	18.2013	3.7443	0.4802
3H-3, 70–72	18.70	655.46	15.9927	2.7673	0.4115
3H-3, 80–82	18.80	657.75	16.9428	3.3986	0.4425
3H-3, 90–92	18.90	660.04	22.0336	4.1004	0.5118
4H-1, 10–12	19.60	676.06	17.0237	2.9000	0.4587
4H-1, 20–22	19.70	678.34	17.6892	3.0047	0.5027
4H-1, 30–32	19.80	680.63	21.8439	5.7804	1.1664
4H-1, 40–42	19.90	682.92	20.4987	3.4801	0.5620
4H-1, 50–52	20.00	685.21	14.5111	2.7915	0.6869
4H-1, 60–62	20.10	687.50	17.6240	3.1209	0.4739
4H-1, 70–72	20.20	689.78	18.2716	3.6813	0.4575
4H-1, 80–82	20.30	692.07	17.4856	3.6005	0.4621
4H-1, 90–93	20.40	694.36	19.0938	4.0759	0.5792

Table 2 (continued).

Core, section, interval (cm)	Depth (mbsf)	Age (ka)	Dry weight (g)	>63-µm weight (g)	>250-µm weight (g)
4H-1, 100–102	20.50	696.65	16.7926	3.3344	0.4933
4H-1, 110–112	20.60	698.94	17.4143	3.5907	0.5054
4H-1, 120–122	20.70	701.22	14.2512	2.4253	0.3654
4H-1, 130–132	20.90	705.80	14.9513	4.3140	0.4861
4H-1, 140–142	21.00	708.09	17.6662	3.1671	0.4861
4H-2, 10–12	21.10	710.38	17.5194	4.2495	1.1751
4H-2, 18–20	21.18	712.21	19.7941	3.7941	0.5023
4H-2, 30–32	21.30	714.95	19.4657	3.8095	0.5628
4H-2, 40–42	21.40	717.24	19.9762	3.9912	0.4233
4H-2, 50–52	21.50	719.53	19.0619	3.8078	0.5319
4H-2, 60–62	21.60	721.82	21.0652	3.7079	0.6981
4H-2, 70–72	21.70	724.10	21.3747	3.8705	0.5191
4H-2, 80–82	21.80	726.39	21.5116	2.9503	0.6118
4H-2, 90–92	21.90	728.68	18.4486	3.6751	1.1586
4H-2, 100–102	22.00	730.97	19.6751	14.1563	3.7986
4H-2, 110–112	22.10	733.26	20.4067	3.9415	0.6113
4H-2, 120–122	22.20	735.54	20.9667	3.7992	0.5625
4H-2, 130–132	22.30	737.83	16.5172	2.8819	0.3797
4H-2, 138–140	22.38	739.66	22.0873	3.9626	0.5913
4H-3, 10–12	22.60	744.70	19.1143	3.6247	0.5140
4H-3, 20–22	22.70	746.98	23.2025	4.6021	0.6094
4H-3, 30–32	22.80	749.27	21.8700	4.8089	0.6799
4H-3, 40–42	22.90	751.56	21.4349	4.5044	0.7586
4H-3, 50–52	23.00	753.85	18.4450	3.0185	0.7903
4H-3, 60–62	23.10	756.14	19.5414	3.7682	0.5150
4H-3, 70–72	23.20	758.42	19.2720	3.8923	0.5620
4H-3, 80–82	23.30	760.71	21.2068	3.9963	0.7920
4H-3, 90–92	23.40	763.00	17.4301	3.5797	0.8838
4H-3, 100–102	23.50	765.29	20.1906	3.5169	0.4924
4H-3, 110–112	23.60	767.58	21.2460	4.0584	0.6693
4H-3, 120–122	23.70	769.86	24.3649	4.9440	0.7899
4H-3, 130–132	23.80	772.15	22.4093	11.1594	1.3096
4H-4, 10–12	24.10	779.02	19.6622	3.7004	0.5208
4H-4, 20–22	24.20	781.78	18.6604	3.1935	0.5446

from ~0.9 to 0.6 Ma) is a central question in Quaternary paleoclimatology (e.g., Prell, 1982; Shackleton and Hall, 1989; Imbrie et al., 1993; Berger et al., 1993; Berger and Jansen, 1994). Marine shelf ice sheets (such as the Barents Sea ice sheet) are thought to play a major role in large-amplitude glacial-interglacial cycles of the late Quaternary (marked by ~100 k.y. periodicity), by allowing major ice build-up on marine shelves and rapid deglaciation (e.g., Broecker and van Donk, 1970; Shackleton and Opdyke, 1973; Vorren et al., 1988; Imbrie et al., 1993). Examination of circum-Arctic ice sheet history can help evaluate the possibility that larger, grounded ice sheets enhanced global $\delta^{18}O$ amplitudes following the middle Quaternary climatic transition. The termination of the overconsolidated section near 670 ka coincides with the well-known increase in the climatic response to the ~100 k.y. period Milankovitch forcing (e.g., Berger et al., 1993). Conventional interpretation of the increased amplitude at the 100 k.y. period includes the supposition that grounded ice sheets became more common in the circum-Arctic during the late Quaternary (Hughes et al., 1977; Prell, 1982; Pollard, 1983; Vorren et al., 1988; Imbrie et al., 1993). Extensive ice buildup on the continental shelves of the Arctic Ocean during glacial intervals may have amplified the 100 k.y. climatic response and enhanced glacial-interglacial $\delta^{18}O$ amplitudes. In this scenario, we might expect to find evidence for grounded marine-based ice sheets such as the Barents Sea ice sheet during glacial intervals after ~800 ka (starting during Stage 22, the first large late Quaternary glacial) and continuing during subsequent glacial intervals to oxygen isotope Stage 2. Evidence exists for several groundings of the Barents Sea ice sheet, probably within the last 800 ka (Vorren et al., 1988), but the age is not well known.

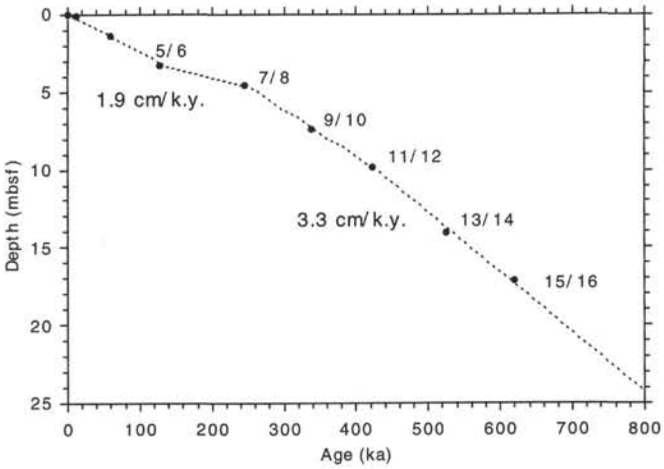

Figure 3. Age vs. depth plot of selected oxygen isotope stage boundaries used in an age model for Hole 910A. Sedimentation rates average ~1.9 cm/k.y. for the 0–245 ka interval and ~3.3 cm/k.y. for the 245–620 ka interval.

Significantly, if the overconsolidated section represents grounding of a Svalbard/Barents Sea ice sheet, then this grounding was clearly most pervasive prior to ~670 ka, and much less so toward the present. Thus, an age of ~670 ka for the top of this section may indi-

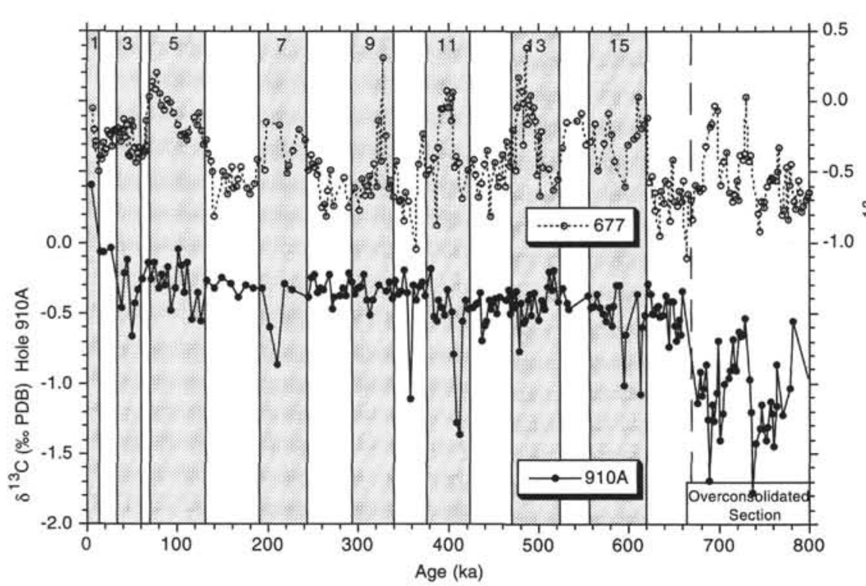

Figure 4. Carbon isotopic records for Hole 910A (based on *N. pachyderma* [sinistrally coiling]) and for Site 677 (based mainly on *Uvigerina*; Shackleton and Hall, 1989), plotted vs. age. Also shown are oxygen isotope stages. Note the general stability of Hole 910A $\delta^{13}C$, except for large variations of ~1‰ prior to ~670 ka.

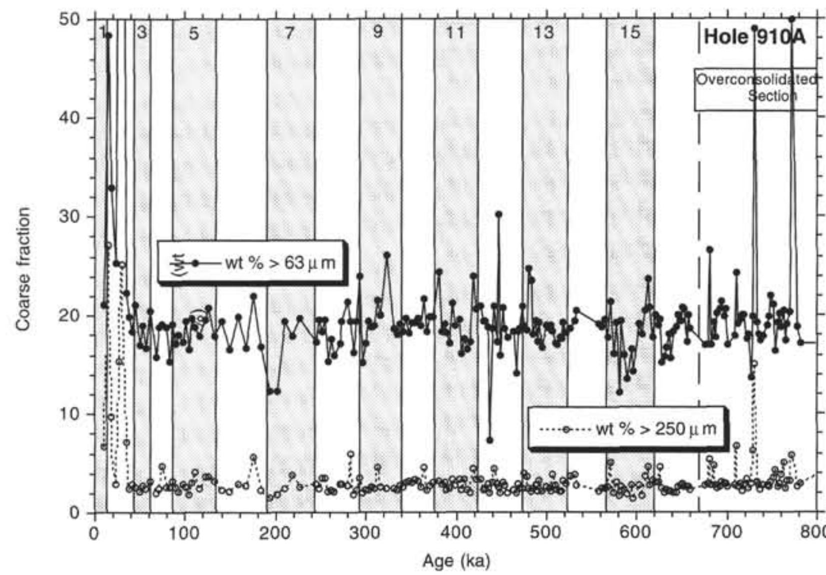

Figure 5. Hole 910A coarse fraction (wt%) vs. age. No significant mean changes in percent >63-µm or percent >250-µm fractions are associated with the overconsolidated section. Also shown are oxygen isotope stages.

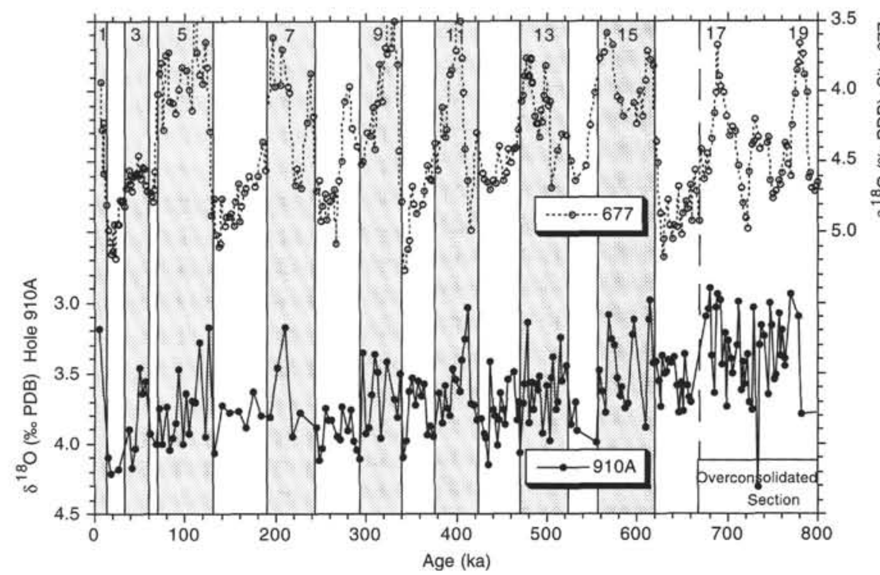

Figure 6. Oxygen isotopic records for Hole 910A (based on *N. pachyderma* [sinistrally coiling]) and for Site 677 (based mainly on *Uvigerina*; Shackleton and Hall, 1989), plotted vs. age. The top of the overconsolidated section at ~19.5 mbsf occurs near the Stage 17/16 boundary (670 ka). Also shown are oxygen isotope stages.

cate that grounded Svalbard/Barents Sea ice sheets did not become more common during the late Quaternary. One possible resolution is that the Barents Sea ice sheet may have undergone a transition from a grounded to a floating, marine-based ice sheet (e.g., Hughes et al., 1977) at this time. Such an ice sheet might still have produced the large glacial-interglacial variations in $\delta^{18}O$ without overcompacting sediment on the Yermak Plateau.

Alternatively, the overconsolidated section may represent increased intensity of ice-rafting prior to ~670 ka. Coarser grained glacial sedimentation might indicate greater ice-rafting through the Fram Strait, or possibly greater erosional capacity of the circum-Arctic ice sheets. The transition near ~670 ka may represent a change from very dynamic ice sheets (at least in the vicinity of the Yermak Plateau) to increased stability of the Arctic cryosphere, including, perhaps, the circum-Arctic ice sheets and the Arctic sea ice. Although the picture is not complete, the available evidence points to larger and/or more dynamic circum-Arctic ice sheets prior to ~670 ka compared to after ~670 ka. Whatever the cause of the overcompaction, the evidence, therefore, seems inconsistent with the idea that larger ice sheets became grounded more commonly in the late Quaternary.

Lastly, I speculate that the termination of ice-sheet grounding on the Yermak Plateau may correspond to a marked change in the character of Svalbard/Barents Sea glaciations during the middle Quaternary, and perhaps to the middle Quaternary climatic transition. Solheim et al. (in press) note a change from net erosion to net deposition on the western Svalbard Margin, which can be traced regionally as the Upper Regional Uncomformity (URU). This transition is attributed to "a shift from thick, eroding glaciers with steep ice profiles, to low profile fast flowing ice streams maintained by an increased amount of interglacial and interstadial sediments" (Solheim et al., in press). Detailed seismic profiling from the western Svalbard Margin to the Yermak Plateau (Solheim et al., unpubl. data) will test the potential link between the URU and the top of the overconsolidated section on the Yermak Plateau.

SUMMARY

Stable isotopic records from ODP Leg 151 Hole 910A based on *N. pachyderma* (s) represent some of the first high-resolution, longterm (middle Quaternary to present) records produced from the Arctic Ocean. The $\delta^{18}O$ data reveal oxygen isotope Stages 1 through 16 (and possibly 17), although the record is complicated by salinity variations. Amplitudes of only ~1‰ suggest salinity changes dampened the glacial-interglacial $\delta^{18}O$ signal throughout the middle to late Quaternary. Termination of a remarkable overconsolidated section below ~19.5 mbsf is dated near the Stage 17/16 boundary (= 670 ka). Large $\delta^{13}C$ fluctuations of >1‰ suggest significant changes in the $\delta^{13}C$ of ΣCO_2 prior to ~670 ka. The large-amplitude variations in $\delta^{13}C$ below ~19.5 mbsf, and the overconsolidated nature of the section, suggest a fundamentally different sedimentary environment. Possible explanations include (1) episodic grounding of a marine-based ice sheet, perhaps derived from the Barents Sea ice sheet and buttressed by Svalbard, that overcompacted the sediment and strongly influenced surface water environments on the Yermak Plateau, and/or (2) coarser grained glacial sedimentation that allowed enhanced compaction during this interval. Whatever the cause of the overcompaction, its termination indicates a major change in Yermak Plateau sedimentation history near the Stage 17/16 boundary (670 ka). This termination may relate to a fundamental change in state of the Svalbard/Barents Sea ice sheets, and to the middle Quaternary climate transition. Further evaluation of late Quaternary circum-Arctic climate history is needed to better understand the role of the Arctic cryosphere in Quaternary climate change.

ACKNOWLEDGMENTS

This work was supported by the JOI/USSSP (151-20794b), along with partial support from NSF (OPP-9423485). I thank the Ocean Drilling Program for inviting my participation on Leg 151; Nao Ahagon for providing samples; D.W. Oppo, W.F. Ruddiman and an anonymous reviewer for helpful reviews; and Melany Manaig, Bhavna Sahi, and Diana Taylor for laboratory assistance.

REFERENCES

Berger, W.H., Bickert, T., Schmidt, H., and Wefer, G., 1993. Quaternary oxygen isotope record of pelagic foraminifers: Site 806, Ontong Java Plateau. *In* Berger, W.H., Kroenke, L.W., Mayer, L.A., et al., *Proc. ODP, Sci. Results,* 130: College Station, TX (Ocean Drilling Program), 381–395.

Berger, W.H., and Jansen, E., 1994. Mid-Pleistocene climate shift: the Nansen connection. *In* Johannessen, O.M., Muensch, R.D., and Overland, J.E. (Eds.), *The Role of the Polar Oceans in Shaping the Global Environment.* Geophys. Monogr., Am. Geophys. Union, 85:295–311.

Broecker, W.S., and van Donk, J., 1970. Insolation changes, ice volumes, and the O^{18} record in deep-sea cores. *Rev. Geophys. Space Phys.,* 8:169–198.

Charles, C.D., and Fairbanks, R.G., 1990. Glacial to interglacial changes in the isotopic gradients of Southern Ocean surface water. *In* Bleil, U., and Thiede, J. (Eds.), *Geological History of Polar Oceans: Arctic Versus Antarctic:* Netherlands (Kluwer Academic), 519–538.

Charles C.D., Wright, J.D., and Fairbanks, R.G., 1993. Thermodynamic influences on the marine carbon isotope record. *Paleoceanography,* 8:691–698.

Dansgaard, W., Johnsen, S.J., Clausen, H.B., and Gundestrup, N., 1973. Stable isotope glaciology. *Medd. Groenl.,* 197:1–53.

Fairbanks, R.G., 1989. A 17,000-year glacio-eustatic sea level record: influence of glacial melting rates on the Younger Dryas event and deep-ocean circulation. *Nature,* 342:637–642.

Fairbanks, R.G., Charles, C.D., and Wright, J.D., 1992. Origin of global meltwater pulses. *In* Taylor, R.E., Long, A., and Kra, R.S. (Eds.), *Radiocarbon After Four Decades:* New York (Springer-Verlag).

Fairbanks, R.G., and Matthews, R.K., 1978. The marine oxygen isotope record in Pleistocene coral, Barbados, West Indies. *Quat. Res.,* 10:181–196.

Hamilton, E.L., 1976. Variations of density and porosity with depth in deep-sea sediments. *J. Sediment. Petrol.,* 46:280–300.

Henrich, R., 1989. Glacial/interglacial cycles in the Norwegian Sea: sedimentology, paleoceanography, and evolution of late Pliocene to Quaternary Northern Hemisphere climate. *In* Eldholm, O., Thiede, J., Taylor, E., et al., *Proc. ODP, Sci. Results,* 104: College Station, TX (Ocean Drilling Program), 189–232.

Hughes, T.C., Denton, G.H., and Grosswald, M.G., 1977. Was there a late Würm Arctic Ice Sheet? *Nature,* 266:596–602.

Imbrie, J., Berger, A., Boyle, E., Clemens, S., Duffy, A., Howard, W., Kukla, G., Kutzbach, J., Martinson, D., McIntyre, A., Mix, A., Molfino, B., Morley, J., Peterson, L., Pisias, N., Prell, W., Raymo, M., Shackleton, N., and Toggweiler, J., 1993. On the structure and origin of major glaciation cycles, 2. The 100,000-year cycle. *Paleoceanography,* 8:699–735.

Imbrie, J., Hays, J.D., Martinson, D.G., McIntyre, A., Mix, A.C., Morley, J.J., Pisias, N.G., Prell, W.L., and Shackleton, N.J., 1984. The orbital theory of Pleistocene climate: support from a revised chronology of the marine $\delta^{18}O$ record. *In* Berger, A., Imbrie, J., Hays, J., Kukla, G., and Saltzman, B. (Eds.), *Milankovitch and Climate* (Pt. 1), NATO ASI Ser. C, Math Phys. Sci., 126: Dordrecht (D. Reidel), 269–305.

Jansen, E., Bleil, U., Henrich, R., Kringstad, L., and Slettemark, B., 1988. Paleoenvironmental changes in the Norwegian Sea and Northeast Atlantic during the last 2.8 m.y.: Deep Sea Drilling Project/Ocean Drilling Program Sites 610, 642, 643, and 644. *Paleoceanography,* 3:563–581.

Johannessen, T., Ravelo, A.C., and Jansen, E., in press. Distribution of carbon and oxygen isotopes in the Greenland, Iceland and Norwegian seas: relationship to water masses, nutrients and circulation. *Mar. Geol.*

Kohfeld, K.E., Fairbanks, R.G., Smith, S.L., and Walsh, I.D., 1994. Decoupling of abundances and geochemical signals of *N. pachyderma* (s.) in marine sediments: evidence from MOCNESS plankton tows. *Eos,* 75:392.

Leg 151 Shipboard Scientific Party, 1994. Farthest north: Ocean drilling in the Arctic Gateway region. *GSA Today,* 5:24–33.

Mix, A.C., and Ruddiman, W.F., 1984. Oxygen-isotope analyses and Pleistocene ice volumes. *Quat. Res.,* 21:1–20.

Morris, T.H., 1988. Stable isotope stratigraphy of the Arctic Ocean: Fram Strait to central Arctic. *Palaeogeogr., Palaeoclimatol., Palaeoecol.,* 64:201–219.

Myhre, A.M., Thiede, J., Firth, J.V., et al., 1995. *Proc. ODP, Init. Repts.,* 151: College Station, TX (Ocean Drilling Program).

Niitsuma, N., Oba, T., and Okada, M., 1991. Oxygen and carbon isotope stratigraphy at Site 723, Oman Margin. *In* Prell, W.L., Niitsuma, N., et al., *Proc. ODP, Sci. Results,* 117: College Station, TX (Ocean Drilling Program), 321–341.

Pollard, D., 1983. A coupled climate-ice sheet model applied to the Quaternary ice ages. *J. Climatol.,* 1:965–997.

Prell, W.L., 1982. Oxygen and carbon isotope stratigraphy for the Quaternary of Hole 502B: evidence for two modes of isotopic variability. *In* Prell, W.L., Gardner, J.V., et al., *Init. Repts. DSDP,* 68: Washington (U.S. Govt. Printing Office), 455–464.

Raffi, I., Backman, J., Rio, D., and Shackleton, N.J., 1993. Plio-Pleistocene nannofossil biostratigraphy and calibration to oxygen isotopes stratigraphies from Deep Sea Drilling Project Site 607 and Ocean Drilling Program Site 677. *Paleoceanography,* 8:387–408.

Ruddiman, W.F., Raymo, M.E., Martinson, D.G., Clement, B.M., and Backman, J., 1989. Pleistocene evolution: Northern Hemisphere ice sheets and North Atlantic Ocean. *Paleoceanography,* 4:353–412.

Shackleton, N.J., Berger, A., and Peltier, W.A., 1990. An alternative astronomical calibration of the lower Pleistocene timescale based on ODP Site 677. *Trans. R. Soc. Edinburgh: Earth Sci.,* 81:251–261.

Shackleton, N.J., and Hall, M.A., 1989. Stable isotope history of the Pleistocene at ODP Site 677. *In* Becker, K., Sakai, H., et al., *Proc. ODP, Sci. Results,* 111: College Station, TX (Ocean Drilling Program), 295–316.

Shackleton, N.J., and Opdyke, N.D., 1973. Oxygen isotope and paleomagnetic stratigraphy of equatorial Pacific core V28-238: oxygen isotope temperatures and ice volumes on a 10^5 year and 10^6 year scale. *Quat. Res.,* 3:39–55.

Shipboard Scientific Party, 1995. Site 910. *In* Myhre, A.M., Thiede, J., Firth, J.V., et al., *Proc. ODP, Init. Repts.,* 151: College Station, TX (Ocean Drilling Program), 221–270.

Solheim, A., Anderson, E.S., Elverhøi, A., and Fiedler, A., in press. Late Cenozoic depositional history of the western Svalbard continental shelf, controlled by subsidence and climate. *Global Planet. Change.*

Spiegler, D., and Jansen, E., 1989. Planktonic foraminifer biostratigraphy of Norwegian Sea sediments: ODP Leg 104. *In* Eldholm, O., Thiede, J., Taylor, E., et al., *Proc. ODP, Sci. Results,* 104: College Station, TX (Ocean Drilling Program), 681–696.

Stein, R., Schubert, C., Vogt, C., and Futterer, D., 1994. Stable isotope stratigraphy, sedimentation rates, and salinity changes in the latest Pleis-

tocene to Holocene eastern central Arctic Ocean. *Mar. Geol.*, 119:333–355.
Thierstein, H.R., Geitzenauer, K., Molfino, B., and Shackleton, N.J., 1977. Global synchroneity of late Quaternary coccolith datum levels: validation by oxygen isotopes. *Geology*, 5:400–404.
Vogt, P.R., Crane, K., and Sudor, E., 1994. Deep Pleistocene iceberg plowmarks on the Yermak Plateau: sidescan and 3.5 kHz evidence for thick calving ice fronts and a possible marine ice sheet in the Arctic Ocean. *Geology*, 22:403–406.
————, 1995. Reply to Comment on "Deep Pleistocene iceberg plowmarks on the Yermak Plateau: sidescan and 3.5 kHz evidence for thick calving ice fronts and a possible marine ice sheet in the Arctic Ocean." *Geology*, 23:477–478.
Vorren, T.O., Hald, M., and Legesbye, E., 1988. Late Cenozoic environments in the Barents Sea. *Paleoceanography*, 3: 601–612.

Date of initial receipt: 7 July 1995
Date of acceptance: 1 December 1995
Ms 151SR-133